IV. CONCLUSIONS

We have presented the results of an extensive LEED study from the various surfaces of Al using the band-structure-matching approach. We have seen explicitly the importance of multiple scattering in interpreting the LEED spectra. It was demonstrated that this method can be successfully used to explain more than qualitatively the nature of the observed spectra. Its advantages are a clear physical meaning and manageable volume of computer calculations. The effects of inelastic scattering may be included phenomenologically in much the same way as in the treatments of McRae, Kambe, and Marcus and Jepsen (see references given in Ref. 1). Its main disadvantage lies in the fact that in its present form it assumes that the penetration depth of an incident electron is large enough to see the three-dimensional band structure. But our pseudo-wave-functions are still a good set of functions with which to carry out the expansion. In addition, it is less suitable for the study of surface layers than, e.g., other methods based on the layer-by-layer calculations.

ACKNOWLEDGMENTS

†Work partially supported by the U. S. Air Force Office of Scientific Research under Grant No. AFOSR 1709-69.

[1]V. Hoffstein and D. S. Boudreaux, Phys. Rev. Letters 25, 8 (1970); 25, 512 (1970).

[2]D. S. Boudreaux and V. Heine, Surface Sci. 8, 426 (1967).

[3]V. Hoffstein and D. S. Boudreaux, Phys. Rev. B 2, 3007 (1970).

[4]W. H. Harrison, *Pseudopotentials in the Theory of Metals* (Benjamin, New York, 1966).

[5]C. Frose-Fisher, thesis, University of British Columbia, 1968 (unpublished).

[6]V. Hoffstein and D. S. Boudreaux, Surface Sci. 21, 99 (1970).

[7]J. B. Pendry, J. Phys. 2, 12 (1969); 2, 2273 (1969).

[8]G. Capart, Surface Sci. 13, 361 (1969).

[9]F. Jona, IBM J. Res. Develop. 14, 444 (1970).

[10]L. De Bersuder (unpublished).

Model Calculations in the Theory of Photoemission*

W. L. Schaich† and N. W. Ashcroft
Laboratory of Atomic and Solid State Physics, Cornell University, Ithaca, New York 14850
(Received 7 December 1970)

Photoemission from several simple models describing the electronic structure of a solid in the presence of a surface is studied. Both nearly free-electron and tight-binding situations are treated, and the yield from the surface states of the latter can be calculated. For a reasonable choice of escape depth, the surface-state yield is roughly of the same magnitude as that from bulk states. With the abundance of different effects, the accent here is placed on understanding the physics involved in the photoemission process rather than on a detailed comparison with experiment. However, several approximate evaluation schemes are also presented and discussed.

I. INTRODUCTION

Photoemission from solids has long been a source of interesting physics,[1] but only recently has its potential as a probe of their electronic structure been pursued.[2-5] Experimental resolution has now improved to the point where rather detailed calculations are necessary for proper analysis of the data. In the last year, two formalisms have appeared which permit a general treatment of the problem.[6,7] One of them, the quadratic-response formalism, is presented along with its independent-particle reduction in Sec. II. The other, a scattering-theory formalism due to Mahan[7] is shown to be equivalent.

Our major purpose in this paper is to examine in detail some computationally simple models of electronic structure in solids and surfaces in order to develop an appreciation for the relevant physics involved in understanding photoemission. In some respects, the models may be too unrealistic for comparison with experiments, but they perform the valuable service of permitting us to identify many basic and important characteristics. We begin in Sec. III with the Sommerfeld model whose photoemissive properties were first properly an-

alyzed by Mitchell.[8] We proceed to the Kronig-Penney model[9] which allows (albeit in a simple fashion) the incorporation of band-structure effects.[6] More importantly, perhaps, it allows us to illustrate two techniques which may be useful in more complex situations, viz., (i) a perturbation method, and (ii) the incorporation of inelastic scattering effects through complex momenta. From these ostensibly nearly free-electron models, we next examine a tight-binding model in Sec. IV. In addition to the well-known bulk states this model admits the possibility of surface electronic states, and we show that these also contribute to the photoemission yield. Indeed, by varying the specification of the surface we are able to exhibit several interesting matrix element effects which contrast quite sharply with the predictions of calculations based on the familiar "constant-matrix-element" approximations. Although care must be taken to distinguish between artifacts of the model and real physical effects the general consequences of surface states seem quite clear. Finally, in Sec. V we summarize our results and discuss the requirements of more realistic calculations.

II. QUADRATIC-RESPONSE FORMALISM

We begin with a brief recapitulation of the quadratic-response theory of photoemission.[6,10,11] Consider a solid (or liquid) located in the half-space $x < 0$. We regard the unperturbed electron states of the system as those determined by the Hamiltonian H_0 which contains the kinetic energy of the electrons and their interaction with the ions, the surface, and themselves. For simplicity we invoke an adiabatic approximation in order to consider the ions as static.

In the presence of the electromagnetic field we have a coupling term

$$H_1 = -(1/c) \int d\vec{r}\, \vec{A}(\vec{r}, t) \cdot \vec{J}(\vec{r})\, e^{\eta t} \quad (\eta = 0^+) , \quad (1)$$

where $\vec{A}(\vec{r}, t)$ is the vector potential of the radiation and $\vec{J}(\vec{r})$ is the current-density operator for the electrons, i.e.,

$$J_\mu(\vec{r}) = \frac{e}{2m} \sum_i [p_\mu^i\, \delta(\vec{r} - \vec{x}^i) + \delta(\vec{r} - \vec{x}^i) p_\mu^i] . \quad (2)$$

By choice of gauge the scalar potential is zero. Notice also that we have not included the contributions from the diamagnetic current,

$$J_\mu^d(\vec{r}, t) = -\frac{e^2}{mc} \sum_i \delta(\vec{r} - \vec{x}^i) A_\mu(\vec{r}, t) , \quad (3)$$

since these contribute (as will any term proportional to A^2 in H_1 by the way) in orders higher than A^2.[6,11] Now, by a straightforward extension of the standard linear-response theory[12] we find for the quadratic response of $\vec{J}(\vec{R})$, where $\vec{R}$ is a macro-

scopic distance outside the material,[11]

$$\langle J_\alpha(\vec{R}, t) \rangle = \left(\frac{1}{\hbar c}\right)^2 \int_{-\infty}^t d\tau_1 \int_{-\infty}^t d\tau_2 \sum_{\mu,\nu} \int d\vec{x}_1$$

$$\times \int d\vec{x}_2\, A_\mu(\vec{x}_1, \tau_1) A_\nu(\vec{x}_2, \tau_2)$$

$$\times \langle\langle\, J_\mu(\vec{x}_1, \tau_1)\, J_\alpha(\vec{R}, t)\, J_\nu(\vec{x}_2, \tau_2)\rangle\rangle . \quad (4)$$

Time dependences of the current-density operators in (4) are determined by H_0 and the symbols $\langle\langle\ \rangle\rangle$ denote a many-body ensemble average. There is *no* linear response and *no* other terms of order A^2 giving an observable result. A preliminary discussion of some of the many-body effects implicit in Eq. (4) has already been given.[6] Our primary concern here is with the independent-particle approximation. Accordingly, we shall, at the outset, neglect the Coulomb interaction between electrons except insofar as it is manifested in (i) a self-consistent screening of the electron-ion potentials, and (ii) an effective depth, imposing a selection on those photoexcited electrons which may actually escape the material.

We specialize to a time dependence $\cos(\omega t)$ in $\vec{A}$. (This is not necessary but it does correspond to the experimental situation in which the radiation is taken to be monochromatic.) With this choice we may easily extract the term for the observed *steady* photoemission, which, in the independent-particle approximation, is[11,13]

$$\langle J_x(\vec{R}) \rangle = \frac{1}{4c^2} \int d\vec{x}_1 \int d\vec{x}_2 \sum_{\mu,\nu} A_\mu(\vec{x}_1) A_\nu(\vec{x}_2) \sum_{m,u,v} n(E_m)$$

$$\times \langle m | j_\mu(\vec{x}_1) | u \rangle \frac{1}{E_m + \hbar\omega - E_u - i\delta'}$$

$$\times \langle u | j_x(\vec{R}) | v \rangle \frac{1}{E_m + \hbar\omega - E_v + i\delta}$$

$$\times \langle v | j_\nu(\vec{x}_2) | m \rangle , \quad\quad \delta, \delta' = 0^+ . \quad (5)$$

Here, now, the j's refer to single-particle current-density operators [see Eq. (2)], and for chemical potential μ, $n(E) = (1 + e^{\beta(E-\mu)})^{-1}$ is a state-occupation factor. Equation (5) therefore describes those electrons that are liberated without any reduction in their energy. The electrons are described by a single-particle Hamiltonian

$$h = (\hbar^2/2m)\nabla^2 + V(\vec{r}) \quad (6)$$

where $V(\vec{r})$ includes the surface potential. To proceed further we clearly need an understanding of the characteristics of the eigenstates of h, and at this point it is convenient after outlining some general results to introduce the physical models.

All the models we treat below have transverse translational symmetry (described by $\vec{a}_2$ and $\vec{a}_3$,

say, with $\vec{a}_2 \cdot \hat{\vec{x}} = \vec{a}_3 \cdot \hat{\vec{x}} = 0$), which immediately allows us to write the eigenfunctions as

$$\psi(\vec{r}) = g(\vec{r}) e^{iK_y y} e^{iK_z z} , \qquad (7)$$

where

$$g(\vec{r} + \vec{a}_2) = g(\vec{r} + \vec{a}_3) = g(\vec{r}) . \qquad (8)$$

Furthermore, well outside the material[14]

$$g(\vec{r}) \to (\alpha e^{ifx} + \beta e^{-ifx}) e^{iK_y y} e^{iK_z z} \quad \text{as } x \to \infty , \qquad (9)$$

where

$$E = (\hbar^2/2m)(f^2 + K_y^2 + K_z^2) \qquad (10)$$

is the energy of the photoelectron and f is the normal component of "exterior" wave vector. By an arbitrary choice we have taken the zero of energy at the *vacuum level*. The two results in Eqs. (7) and (9) will allow us to cast Eq. (5) into a more familiar form. Let us concentrate on the factor

$$F = \frac{1}{E_m + \hbar\omega - E_u - i\delta'} \langle u | j_x(\vec{R}) | v \rangle \frac{1}{E_m + \hbar\omega - E_v + i\delta} .$$

If we average the current density (and hence F) over a transverse macroscopic region of area $L_y L_z$ (corresponding to the process involved in physically detecting the current), we deduce the requirement of transverse momentum conservation between the states $|u\rangle$ and $|v\rangle$. Next, we note an identity, which may be proved by integration with respect to $f^{(v)}$, namely,

$$\frac{e^{if^{(v)}\vec{R} \cdot \hat{\vec{x}}}}{E_m + \hbar\omega - E_v + i\delta} = - 2\pi i \,\delta(E_m + \hbar\omega - E_v)$$

$$\times \, e^{if^{(v)}\vec{R} \cdot \hat{\vec{x}}} \theta(f^{(v)}) , \qquad (11)$$

where the θ function requires the normal momentum to be positive. This restriction allows only outgoing waves to contribute to the photocurrent. In addition, from Eq. (11) and its complex conjugate, we may readily deduce that the states $|u\rangle$ and $|v\rangle$ have the same energy. Since in the simple models we treat below there are only two linearly independent states for each choice of transverse momentum and energy (greater than zero) and moreover one of these can always be chosen to contain no outgoing waves outside the material, we conclude that the states $|u\rangle$ and $|v\rangle$ may be taken as identical. In this case it follows that if we were to sum the averaged factor F over states $|u\rangle$ and $|v\rangle$ we would find

$$\sum_{u,v} (F)_{av} = \frac{1}{L_y L_z} \sum_{K_y, K_z} \int \frac{df^{(u)}}{2\pi} \int \frac{df^{(v)}}{2\pi} (F)_{av}$$

$$= \frac{1}{L_y L_z} \sum_{K_y, K_z} \int \frac{df^{(u)}}{2\pi} [2\pi i \,\delta(E_m + \hbar\omega - E_u)] \left(\frac{e\hbar f}{m}\right)$$

$$\times \int \frac{df^{(v)}}{2\pi} [- 2\pi i \,\delta(E_m + \hbar\omega - E_v)]$$

$$= \frac{1}{L_y L_z} \sum_{K_y, K_z} \frac{e\hbar f}{m} \left(\frac{m}{\hbar^2 f}\right)^2$$

$$= \frac{1}{L_y L_z} \sum_{K_y, K_z} \int \frac{df}{2\pi} e \frac{2\pi}{\hbar} \,\delta(E_m + \hbar\omega - E) . \qquad (12)$$

We have assumed here that the coefficient (or weight) of the outgoing wave is unity, and that the states are normalized to a δ function on the outgoing momentum. (These requirements will be satisfied in Secs. III and IV.) Our formal manipulation in Eq. (12) allows us to rewrite Eq. (5) as

$$(\langle J_x(\vec{R}) \rangle)_{av} = \langle J_x(\vec{R}) \rangle = \frac{e}{L_y L_z} \frac{2\pi}{\hbar} \sum_{m, \tilde{u}} n(E_m)$$

$$\times | \langle m | H' | \tilde{u} \rangle |^2 \,\delta(E_m + \hbar\omega - E_u) , \qquad (13)$$

with

$$H' = - (1/c) \int d\vec{x} \sum_\mu \tfrac{1}{2} A_\mu(\vec{x}) j_\mu(\vec{x}) . \qquad (14)$$

The notation $|\tilde{u}\rangle$ emphasizes the special nature of the final state to which transitions are allowed in photoemission. It is evident from the "golden rule" form of Eq. (13) that the photocurrent may also be represented as a transition rate. However, the precise nature of the final state required in the sum only follows from a careful analysis of the response formalism.

We now turn to the alternative view of photoemission as a scattering process[15] (incoming photons, outgoing photoelectrons) and show that the resulting formalism leads to results identical to those above.[7] In the scattering approach the nature of the final state is determined by examining the asymptotic form of a Green's function.[7,15] To illustrate the equivalence of the two approaches (quadratic response and scattering theory) in the problem at hand, let us explicitly write the sum over $|\tilde{u}\rangle$ in Eq. (13) as

$$\sum_{\tilde{u}} \to \int \frac{df}{2\pi} \int \frac{dK_y}{2\pi} \int \frac{dK_z}{2\pi} . \qquad (15)$$

Now (i) use the normal momentum integral to eliminate the energy δ function:

$$\int df \,\delta(E_m + \hbar\omega - E_{\tilde{u}}) = m/\hbar^2 f ; \qquad (16)$$

and (ii) change variables in the transverse momentum integrations to the external angles of emission, θ and φ (which are measured from the surface normal):

$$\int \frac{dK_y}{2\pi} \int \frac{dK_z}{2\pi} \rightarrow \frac{1}{(2\pi)^2} \int \frac{2mE}{\hbar^2} \cos\theta \, d\Omega$$

$$(d\Omega = \sin\theta \, d\theta \, d\varphi) \ . \quad (17)$$

Incorporating these changes we find

$$\langle J_x(\vec{R}) \rangle = \frac{e}{L_y L_z} \frac{m}{(2\pi)^2} \frac{1}{\hbar^3} \int d\Omega \sum_m n(E_m)$$

$$\times |\langle m|H'|\tilde{u}\rangle|^2 \left(\frac{2mE}{\hbar^2}\right)^{1/2} , \quad (18)$$

which is one of Mahan's[7] basic results. A more general statement of the equivalence is that the vacuum "incoming waves" of scattering theory[15,16] diagonalize $(F)_{av}$, when it is viewed as an operator. (This observation permits a generalization of the analysis given above.[11])

III. MITCHELL AND KRONIG-PENNY MODELS

We have numerically evaluated expressions for the photoemission in the context of several simple models which are outlined in turn. To start, let us treat Mitchell's simplest model[8]: free electrons in a semi-infinite box. For the Hamiltonian h we have

$$h = -(\hbar^2/2m) \nabla^2 + V(x) , \quad (19)$$

where the only structure in $V(x)$ is a step discontinuity of height V_0 at the surface $x = 0$. The eigenstates above the vacuum level can be chosen as[11]

$$\psi_1(\vec{r}) = |\tilde{u}\rangle = \left(e^{ifx} + \frac{f - K_x}{f + K_x} e^{-ifx}\right) e^{iK_y y} e^{iK_z z} \quad x > 0$$

$$= \left(\frac{2f}{f + K_x}\right) e^{iK_x x} e^{iK_y y} e^{iK_z z} , \quad x < 0$$

$$(20)$$

$$\psi_2(\vec{r}) = \frac{2K_x}{f + K_x} \left(\frac{f}{K_x}\right)^{1/2} e^{-ifx} e^{iK_y y} e^{iK_z z} \quad x > 0$$

$$= \left(\frac{f}{K_x}\right)^{1/2} \left(e^{-iK_x x} + \frac{K_x - f}{f + K_x} e^{iK_x x}\right) e^{iK_y y} e^{iK_z z} ,$$

$$x < 0$$

$$(21)$$

where

$$K_x > 0, \quad f > 0, \quad (22)$$

and

$$0 < E_{1,2} = \frac{\hbar^2}{2m} (f^2 + K_y^2 + K_z^2)$$

$$= \frac{\hbar^2}{2m} (K_x^2 + K_y^2 + K_z^2) - V_0 . \quad (23)$$

It is easily verified that these states are ortho-normalized,[11]

$$\langle \psi_1 | \psi_1' \rangle = \langle \psi_2 | \psi_2' \rangle = (2\pi)^3 \delta(f - f')$$

$$\times \delta(K_y - K_y') \delta(K_z - K_z') , \quad (24)$$

$$\langle \psi_1 | \psi_2 \rangle = 0 . \quad (25)$$

Further, the state ψ_2 contains no outgoing waves outside the material and consequently makes no contribution to photoemission (hence our identification of $|\tilde{u}\rangle$ with ψ_1).

For an energy below the vacuum level, there is only one state for each choice of transverse momenta (K_y and K_z):

$$\psi(\vec{r}) = |m\rangle = \frac{2ik_x}{p + ik_x} e^{-px} e^{ik_y y} e^{ik_z z} \quad x > 0$$

$$= e^{-ik_x x} + \frac{ik_x - p}{ik_x + p} e^{ik_x x} e^{ik_y y} e^{ik_z z} ,$$

$$x < 0 \quad (26)$$

where

$$k_x > 0, \quad p > 0 , \quad (27)$$

and

$$0 > E = \frac{\hbar^2}{2m} (-p^2 + k_y^2 + k_z^2) = \frac{\hbar^2}{2m} (k_x^2 + k_y^2 + k_z^2) - V_0 . \quad (28)$$

This state is normalized so that

$$\langle \psi | \psi' \rangle = (2\pi)^3 \delta(\vec{k} - \vec{k}') . \quad (29)$$

As for the momentum matrix elements in Eq. (13), their evaluation is straightforward if we ignore any spatial dependence of the vector potential. This approximation is made for the sake of simplicity; a realistic treatment of the vector potential unfortunately appears to be both difficult and necessary, at least insofar as "surface effects" may be important.[17,18] We will return to this point in Sec. V. The consequence of the approximation is that we may now write

$$H' = -\left(\frac{eA}{2mc}\right) \frac{\hbar}{i} \vec{\epsilon} \cdot \vec{\nabla}, \quad |\vec{\epsilon}| = 1 \quad (30)$$

where we have introduced here the polarization vector $\vec{\epsilon}$ of the vector potential. The matrix elements follow immediately from the identity[19]

$$\langle m|\vec{\epsilon} \cdot \vec{\nabla}|\tilde{u}\rangle = \langle m|\vec{\epsilon} \cdot (\vec{\nabla} V)|\tilde{u}\rangle \left(\frac{1}{\epsilon_{\tilde{u}} - \epsilon_m}\right) , \quad (31)$$

where, for a step potential

$$\vec{\nabla} V = \hat{x} V_0 \, \delta(x) . \quad (32)$$

It immediately follows that there is no photoemission if the light is at normal incidence to the step barrier. Collecting these results into Eq. (13) we find

$$\langle J_x(\vec{R})\rangle = \left(\frac{eA \cdot \hat{\vec{x}}}{\hbar c}\right)^2 \left(\frac{V_0}{2\pi^3 m\ \omega^2}\right)$$

$$\times \int_{k_x > 0} d^3k\ n(\epsilon_k) \frac{k_x^2}{(f+K_x)^2} \frac{e\hbar f}{m} \ . \tag{33}$$

Apart from a factor of 2 this is the result of Mitchell.[8] (We agree with Adawi's[15] comment on the factor of 2.) Only a slight extension of the above result is necessary to obtain the result of Makinson[20] for an arbitrary surface barrier. Mahan[7] has shown how Eq. (33) may be further reduced.

In order to introduce some elements of band structure we next consider a Kronig-Penney model terminated by a step barrier.[6,9] The potential in Eq. (19) is replaced in this model by

$$V(x) = 0 \qquad\qquad\qquad x > 0$$

$$= \frac{\hbar^2}{2m} \frac{2P}{a} \sum_{n=0}^{\infty} \delta(x + na + b) - V_0 \ , \quad x < 0 \ . \tag{34}$$

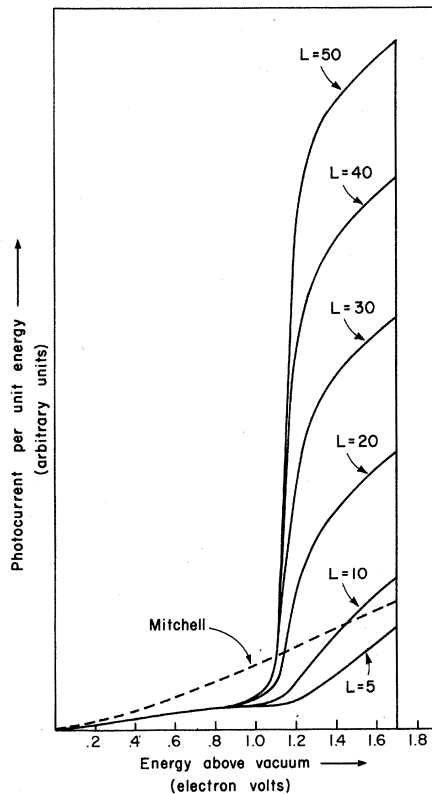Here P is a dimensionless parameter which con-

FIG. 1. EDC's for modified Kronig-Penney model parametrized by effective depth L: solid curves. EDC for Mitchell model: dashed curve. (See text for explanation of parameters.)

trols the strength of the periodic potential. The parameters a and b describe the lattice spacing and the surface termination, respectively. (Again, light of normal incidence yields no photoeffect.) By way of example we choose the parameters of the model to represent, as near as possible, the $\langle 110 \rangle$ planes of sodium: The model possesses the same spacing in the x direction and has the same Fermi energy,[21] first band gap, and photoelectric threshold. Accordingly (assuming the temperature to be near 0 °K) we take[22] the lattice spacing a as 5.65 a.u., the Fermi energy as 3.24 eV, the band gap as 0.50 eV ($P \approx 0.30$), and the work function[23] as 2.3 eV. Since the solutions of the Kronig-Penney model are well known[9,24] we merely assert that the eigenfunctions can be taken to have the same form as those in Eqs. (20), (21), and (26). The computation of the matrix elements is complicated somewhat by the need to introduce a damping factor (of the form $e^{+x/La}$) into the integration over negative x. At this stage, the factor is purely *ad hoc* and limits the contribution of the "volume" effect, which arises when the excited electron absorbs momentum from the "lattice." Its physical origin is clear, however, being a combination of the damping of the vector potential as it penetrates the material and the damping (by the electron gas) of the photoexcited electrons as they travel toward the surface.[6] In metals the latter process is dominant over the energy range of interest here. One final point is that aside from the damping factor we again ignore the spatial dependence of the vector potential.

We now turn to a discussion of some of the numerical results of the modified Kronig-Penney model. In Fig. 1 we have plotted energy distribution curves (EDC's) for a photon energy of 4 eV (1.7 eV above threshold).[25] The curves are parametrized by L, which is approximately the number of planes below the surface from which electrons are allowed to emerge. The growth of a "volume effect" as L increases is apparent. However, since the "volume" and "surface" effect, to the extent that they can be separated, both occur within the matrix element of Eq. (13), and since the photocurrent is determined by the absolute square of this quantity, the two effects must interfere with each other. In this regard it is pertinent to note that Mahan[7] has shown using alternative models, that this interference may not always occur. On physical grounds (mainly the normal expectation of unavoidable surface roughness), we feel that some interference will always be present. In Fig. 1 interference is exhibited for $L = 5$ or 10 [the EDC's of Mitchell's pure surface effect are roughly proportional[7,26] to $E^{3/2}$ where E is the energy above the vacuum (the coordinate of the abscissa of Fig. 1)]. This last point is illustrated by the dashed
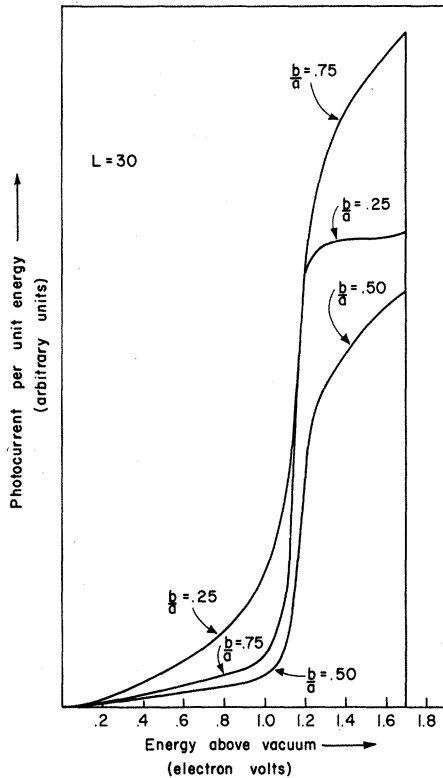
FIG. 2. EDC's for modified Kronig-Penney model parametrized by position of matching plane [b of Eq. (34)].

normal. There is no dependence on the azimuthal angle since our model Hamiltonian has cylindrical symmetry about the surface normal. The energy of the photoelectrons has been fixed at 1.4 eV. If we were to integrate with respect to $\sin\theta\,d\theta$ we would obtain the points on the curves in Fig. 1 above $E = 1.4$ eV. Mitchell's model [Eq. (33)] of a pure surface effect predicts essentially a $\cos^2\theta$ dependence[7,26] (as illustrated by the dashed line). At low L we can see how the volume effect both adds to ($\theta < 25°$) and subtracts from ($\theta > 25°$) the surface effect. Another feature of the curves is that as the effective depth L increases, the electrons excited by the volume effect are emitted at a fixed angle ($\approx 25°$ here). This effect has been predicted,[3,7] but note that in the physical range of L values the distribution is still quite broad. We also find that its width depends on the energy of observation.

As a check of our numerical work we have evaluated the photoemission of this model using perturbation theory. The procedure is to first ignore the presence of the lattice potential in the evaluation of Eq. (13) except within the matrix elements where the transformation of Eq. (31) is used.[7,10] Thus we use the wave functions of Eqs. (20) and (26) and the free-electron dispersion relation but allow volume absorption through $\vec{\nabla}V$. The results we

curve in Fig. 1 which is the EDC predicted by Eq. (33). Another way to demonstrate the importance of the surface is to vary the position of the matching plane, i.e., vary the parameter b [Eq. (34)]. The curves of Fig. 1 were for $b = a/2$. In Fig. 2 we fix L equal to 30 and vary b, obtaining as shown, a strong variation. At first glance one might expect the ratio of surface to volume effects to be $1/L \approx 3\%$. However, this estimate ignores the relative oscillator strength of the two effects: For our model

$$V_0 = 5.54 \text{ eV} > 0.26 \text{ eV} = \frac{\hbar^2}{2m}\frac{2P}{a^2} , \qquad (35)$$

which observation, coupled with Eq. (31), explains why the EDC's are so sensitive to the surface condition. Much larger values of L are necessary in order to ensure *complete* dominance of the volume effect. Our choice of L is not unreasonable if one considers, for example, the experiments of Piepenbring[27]; in fact, the later work of Smith and Spicer[23] indicates that L may be smaller still.

In Fig. 3 we plot some angular distribution curves (ADC's) where again the interference is apparent. The ordinate is proportional to the photocurrent per solid angle of emission; the abscissa measures the angle θ away from the surface
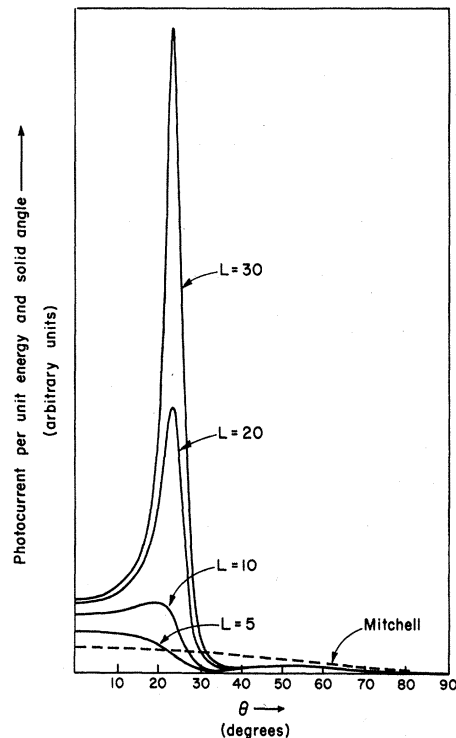

FIG. 3. ADC's for modified Kronig-Penney model parametrized by effective depth L: solid curves. ADC for Mitchell model: dashed curve.

obtain are practically the same as those of the exact evaluation. It is worth pointing out that because of the simplifications in the wave functions the calculations are much more rapidly completed.

An interesting comparison is possible within this model. Mahan[7] has shown that in the volume-effect limit one can obtain from the perturbation approach a closed form expression for the EDC. Applying his method to our model here, we find that the EDC should be rectangular in shape with a height that scales with L. In Fig. 4 we compare this exact volume-effect prediction with our calculations based on the perturbation method. Interference is clearly apparent. Note, however, that the relative disagreement decreases with L but still is substantial for a realistic value of effective depth.

In an attempt to put the choice of L on a more systematic basis, we adapt the procedure of Jones and Strozier in their calculation of low-energy-electron-diffraction (LEED) intensities.[28] We fit to an algebraic curve the data of Lundqvist[29] for the imaginary part of the self-energy $\text{Im}\Sigma$ of an electron gas at a density appropriate to sodium ($r_s = 4$). Then we solve the equation[28]

$$\frac{\hbar^2}{2m}\left[\text{Re}(K_x) + i\,\text{Im}(K_x)\right]^2 = E - \frac{\hbar^2}{2m}\left(K_y^2 + K_z^2\right)$$

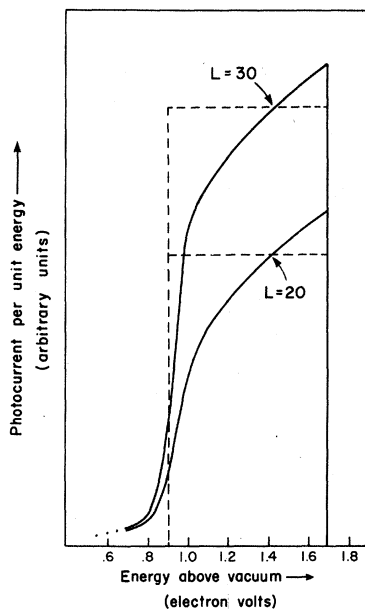$$+ i\,\text{Im}[\Sigma(E)] \qquad (36)$$

FIG. 4. EDC's for the modified Kronig-Penney model evaluated in perturbation theory for two values of the effective depth L: solid curves. EDC's for same model evaluated in volume-effect limit for the same two values of L: dashed curves.
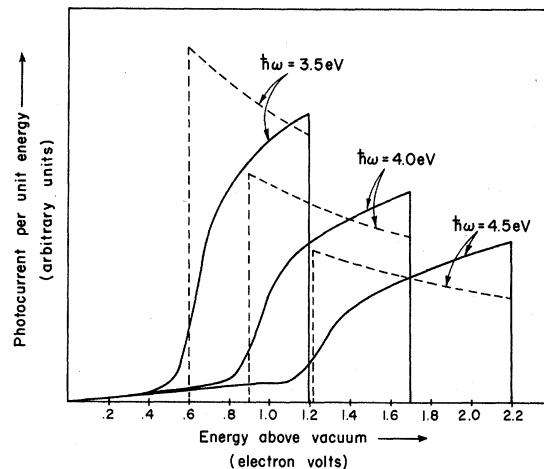
FIG. 5. EDC's for modified Kronig-Penney model evaluated in perturbation theory using complex momenta: solid curves. Also plotted is the volume-effect limit prediction of this model: dashed lines.

to lowest order in $\text{Im}\Sigma$ to obtain for the complex normal momentum inside the material:

$$\text{Re}(K_x) = \left(\frac{2m}{\hbar^2}\right)^{1/2}\left(E - \frac{\hbar^2}{2m}\left(K_y^2 + K_z^2\right)\right)^{1/2} , \qquad (37)$$

$$\text{Im}(K_x) = \frac{1}{La} = \text{Im}\Sigma(E)\bigg/\left(\frac{\hbar^2}{m}\text{Re}(K_x)\right) . \qquad (38)$$

Using these results we can now follow the development of the EDC's as photon energy is varied.[30] Figure 5 illustrates this possibility: The decrease in the magnitude of the yield arises from the increased scattering of the higher-energy photoelectrons. The curves predicted for a pure volume effect have lost their rectangular shape for exactly the same reason. We note that our results are consistent with the discussions of several authors[23,31] who find that experimental EDC's change both in energy and width in the manner predicted by a volume-effect model but that the *shape* of the curves is not correctly described. We must caution, however, that (i) the usual experimental arrangement—light at normal incidence on a multicrystalline surface—is quite different from the assumptions of our model; and (ii), as $\text{Im}(\Sigma)$ increases our whole procedure (based on a single-particle formalism) becomes questionable. In the curves of Fig. 5 $\text{Im}(\Sigma)$ is always less than 20% of the Fermi energy.

IV. GOODWIN MODEL

The last model we treat is that of Goodwin[32] who examined the s-wave tight-binding states of a bounded simple-cubic crystal. We assume that a {100} face is exposed to the vacuum. The model

admits both bulk and surface states and we shall use these solutions for the states below the vacuum level. The explicit wave functions and dispersion relations are the following[32]:

Case I: Bulk states.

$$\psi_B(\vec{r}) = \sum_{l=0}^{-\infty} \sum_{m,n=-\infty}^{\infty} e^{ik_y ma} e^{ik_z na} \left[e^{-ik_x la} - B_{k_x} e^{ik_x la} \right]$$

$$\times \varphi(\vec{r} - \vec{R}_{l,m,n}) , \qquad (39)$$

where

$$B_{k_x} = \frac{\epsilon/\gamma + \cos k_x a - i \sin k_x a}{\epsilon/\gamma + \cos k_x a + i \sin k_x a} , \quad k_x > 0. \qquad (40)$$

Here the lattice parameter is a, $\vec{R}_{l,m,n}$ specifies the lattice sites, and φ is the localized orbital normalized to

$$\langle \varphi | \varphi \rangle = a^3 , \qquad (41)$$

so that

$$\langle \psi_B | \psi_B' \rangle = (2\pi)^3 \, \delta(\vec{k} - \vec{k}') . \qquad (42)$$

The parameter $\epsilon > 0$ is a measure of the potential change at the surface while $\gamma > 0$ is the usual overlap integral common in the tight-binding method:

$$E = E_0 - 2\gamma (\cos k_x a + \cos k_y a + \cos k_z a) . \qquad (43)$$

Case II: Surface states.

$$\psi_s(\vec{r}) = \sum_{l=0}^{-\infty} \sum_{m,n=-\infty}^{\infty} e^{ik_y ma} e^{ik_z na} (-)^l e^{l\mu} \, \varphi(\vec{r} - \vec{R}_{l,m,n})$$

$$\times \left[1 - \left(\frac{\gamma}{\epsilon} \right)^2 \right]^{1/2} \left(\frac{1}{a} \right)^{1/2} , \qquad (44)$$

where

$$\mu = \ln \epsilon/\gamma , \qquad (45)$$

and ϵ/γ must be greater than unity in order for the surface ("Tamm") state to exist. With φ normalized as in Eq. (41),

$$\langle \psi_s | \psi_s' \rangle = (2\pi)^2 \, \delta(k_y - k_y') \, \delta(k_z - k_z') . \qquad (46)$$

The state is split off from the top of the band

$$E = E_0 + 2\gamma \cosh \mu - 2\gamma (\cos k_y a + \cos k_z a) . \qquad (47)$$

For the final state in the photoexcitation we use the free-electron wave function of Eq. (20) with the matching plane situated a distance b beyond the outermost layer of atoms. To simplify the computation of the matrix elements, we neglect the spatial dependence of the vector potential (aside, again, from using an exponential damping factor) and write the orbital φ as

$$\varphi(\vec{r}) = \alpha^{3/2} \, e^{-|\alpha x/a|} e^{-|\alpha y/a|} e^{-|\alpha z/a|} , \quad \alpha \approx 4 \qquad (48)$$

so that a partial Fourier transform may be taken in closed form. We choose the parameters a, E_0, γ,

and V_0 so that the model resembles the basic features of copper.[33] Thus

$$a = 4.31 \text{ a.u.} \qquad (49)$$

and the Fermi energy is

$$E_F + V_0 = \frac{\hbar^2}{2m} \left(\frac{3}{\pi} \right)^{2/3} \left(\frac{\pi}{a} \right)^2 = 7.0 \text{ eV} . \qquad (50)$$

Further

$$E_0 + V_0 = 3.4 \text{ eV} , \qquad (51)$$

$$\gamma = 0.25 \text{ eV} , \qquad (52)$$

and thus the bandwidth is 3.0 eV. Finally[34]

$$V_0 = 11.5 \text{ eV} , \qquad (53)$$

or, if we have a cesium-coated surface, 8.5 eV. The energy-dependent damping length is determined by[34]

$$1/L = 0.025 + \alpha (E - E_F)^2 , \qquad (54)$$

where the first term represents the light damping and the second the damping due to electron-electron scattering. The coefficient α is determined by requiring[34,35]

$$\alpha (8.6 \text{ eV})^2 = \tfrac{1}{6.1} . \qquad (55)$$
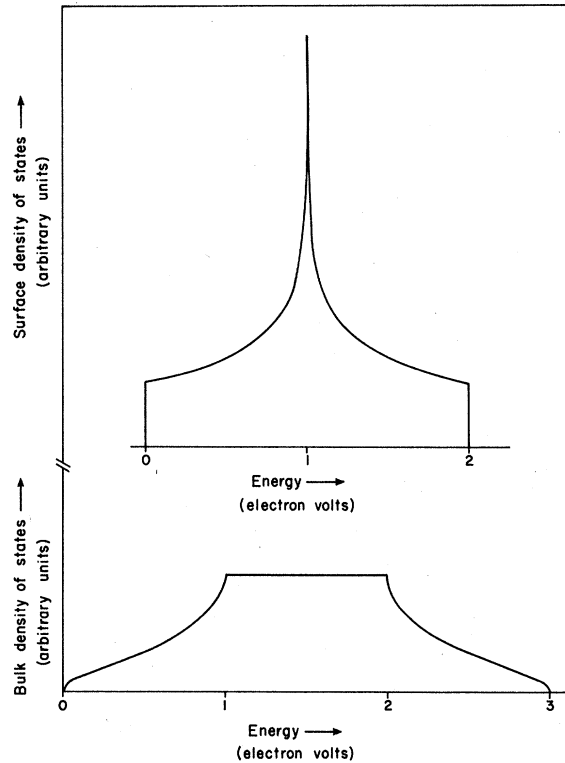

FIG. 6. Surface and bulk densities of states for Goodwin model. The zeros of energy are simply chosen for convenience; the units for the two curves are different.

We note that in this model photoemission results from light incident at *any* angle but that excitations from transverse and normal components do not interfere; we shall present our results as at either grazing incidence or normal incidence. The computation of the matrix elements is straightforward but lengthy. As for the integrations over available states, the explicit form of the dispersion relations allows us to project the energy surfaces onto various planes and thereby avoid the statistical errors of an integration over an energy δ function.[34] As an illustration of the precision of the integration scheme we present in Fig. 6 the densities of states for both the bulk and surface states. The singularity in the surface density of states is logarithmic which is not unexpected. To summarize the model, we have, admittedly, some artificial features but by way of compensation there are available easily controlled parameters whose physical significance and consequences are clear. It follows that we may hope to uncover most of the relevant physics without performing too extensive a calculation.

Let us begin be examining in Fig. 7 the changes in the EDC's as the photon energy is increased. The barrier height V_0 has been set at 11.5 eV and we consider light at grazing incidence. The
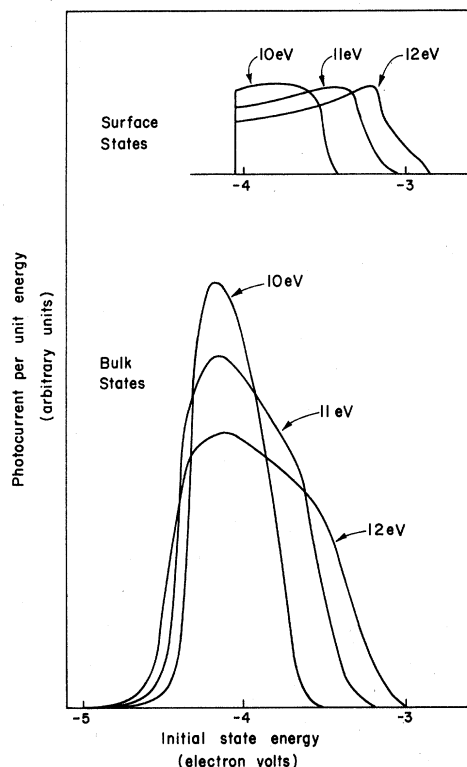

FIG. 7. EDC's for Goodwin model parametrized by photon energy. The curves for both surface and bulk initial states are plotted in the same units and normalized to unit photon flux at grazing incidence.
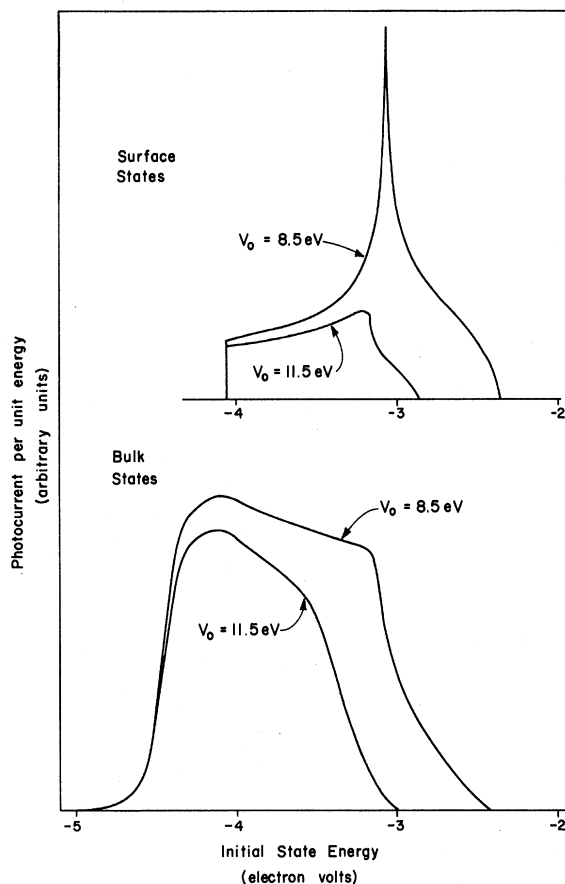

FIG. 8. EDC's for Goodwin model plotted as in Fig. 7. The photon energy is 12 eV; the surface-barrier height is lowered to simulate cesiation of the surface.

parameters b and ϵ/γ are $a/2$ and 1.5, respectively. We have plotted the yield (in arbitrary units) against the initial energy; the zero of energy is at the Fermi level. Yields from the surface and bulk states have been plotted separately for clarity. Note how, with increasing photon energy, the surface-state yield becomes a large fraction of the total due to the enhanced scattering of the bulk-state photoelectrons. The ratio of ϵ/γ that we have chosen corresponds to an intrinsic depth of the surface state of approximately 2.5 layers [Eqs. (44) and (45)]; hence all photoelectrons from these states (with sufficient normal momentum after excitation) may escape so long as the damping length [L of Eq. (54)] remains greater than 2.5. The substantially constant magnitude of the surface-state yield arises from a balance between decreasing oscillator strength and increasing phase space. Eventually the former will dominate.

In Fig. 8 we simulate cesiation of the surface by lowering the surface barrier to 8.5 eV.[5,34] Both curves are for a photon energy of 12 eV. Most striking is the fact that the logarithmic singularity
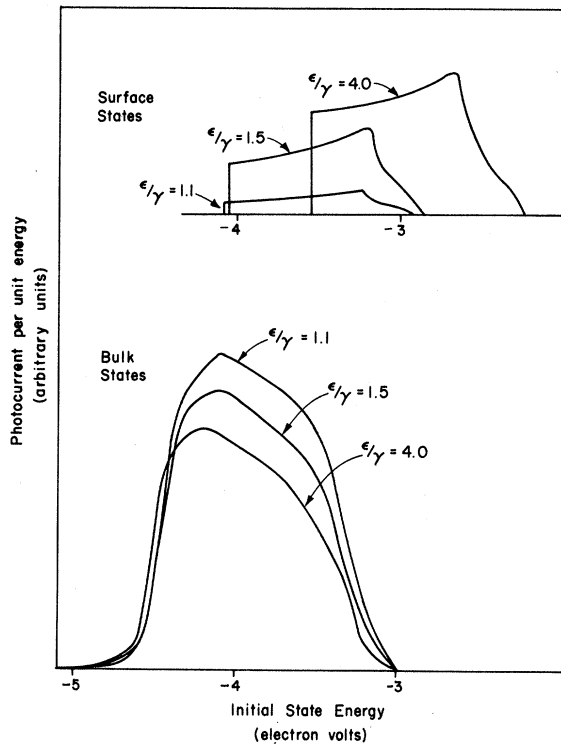
FIG. 9. EDC's for Goodwin model plotted as in Fig. 7. The photon energy is 12 eV; the specification of the surface potential is varied through the parameter ϵ/γ.

in density of surface states is now apparent. Experimentally it would, of course, be difficult to distinguish this structure from bulk-state structure, without varying surface conditions.

A further interesting feature of the surface-state yield may be deduced from Fig. 9 where at fixed photon energy we vary the intrinsic depth of the surface state: For $\epsilon/\gamma = 1.1$ this depth is approximately ten layers while for $\epsilon/\gamma = 4.0$ it is less than one layer. We see that the less the surface state penetrates, the more it contributes to the photoelectric yield. At first sight this is surprising but the reason for this behavior arises from the normalization factor $[1 - (\gamma/\epsilon)^2]^{1/2}$ of Eq. (44) and the interplay between the intrinsic depth of the states and the damping length. Relatively short damping lengths (5–10 layers here) obviously require the detected photoelectrons to originate from near the surface, but, as the intrinsic depth increases, the normalization factor decreases the magnitude of the surface-state wave function in the surface region and hence actually decreases the yield. We note in passing that the variation of ϵ/γ also affects the bulk-state yield. This, too, is a matrix element effect that arises from the presence of the surface. From Eq. (40) we see that increasing ϵ/γ makes B_{k_x} tend to unity, which in turn places a node at the surface and consequent-

ly reduces the yield. We shall return to this point later.

We have not discussed the shift (with ϵ/γ) in energy of the surface-state yield because the energy position of the surface states is not realistically treated in this model.[36] Nor is it clear whether surface states of the sort we are using here even exist in metals. However, the existence of surface states of a different nature has been recently predicted for copper and nickel.[37,38] Unfortunately a proper calculation of photoemission from such states is presently too involved since it must require the wave functions and dipole matrix elements throughout the entire zone in reciprocal space rather than just eigenvalues at symmetry points. Nonetheless it is reasonable to expect that Goodwin's model allows us to represent (with few parameters) the essential features of the surface-state wave function, even though the eigenvalue and physical origin of the state may not be correct.

It is in this spirit that we now examine the effect of varying the position of the matching plane. In Fig. 10 we have ignored the zero of energy in plotting the surface EDC's and have included only the central portion of the EDC's from bulk states. We vary the value of b between $a/4$ and[39] $a/2$ and the ratio ϵ/γ between 1.1, 1.5, and 4.0; all curves are for the same incident photon energy of 12 eV. The most obvious and quite striking feature is that surface- and bulk-state yields are opposite in their
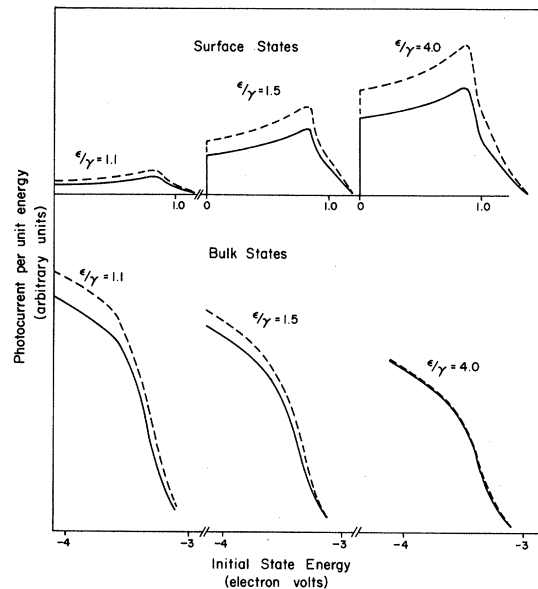

FIG. 10. EDC's for Goodwin model plotted as in Fig. 7 except for the neglect of the zero of energy in the surface state EDC's and the presentation of only the central portion of the bulk-state EDC's. The parameter b is $a/2$ for the solid curves and $a/4$ for the dashed curves.

sensitivity to ϵ/γ and b. For large ϵ/γ the surface states are strongly localized at the surface, while the bulk states have a node there. On the other hand, for small ϵ/γ the surface states penetrate far into the material while the bulk states extend up to the surface. Though these features of the eigenstates may not be universal, their consequences in the phenomenon of photoemission are clear.

We now turn to the photoemissive yield that results from light at normal incidence. We see from Fig. 11 (which is to be contrasted with the 12-V curve of Fig. 7) that (i) there is an order-of-magnitude decrease in the yield, and (ii) a considerable "reshaping" has occurred. The reason underlying these changes arises from the form of the final-state wave function: In order to escape the material a photoelectron usually has more normal momentum than transverse momentum, in the energy range of interest here. Light at normal incidence, which couples through the transverse momentum, therefore finds a lower oscillator strength. If we locate the energy range where the momentum is mostly normal, there we also find considerable reshaping of the EDC. As expected for this model, the EDC's for light at normal incidence show less sensitivity to the position of the matching plane.

The final point we shall discuss is the general shape of the EDC's. The data that we have pre-

FIG. 12. EDC's for Goodwin model various approximations plotted as in Fig. 7 for a photon energy of 12 eV. Full curve: exact result; dashed curve: density-of-states approximation; and dotted curve: joint-density-of-states approximation.

sented so far all show a resemblance to the densities of states of Fig. 6, though the distortion is severe in Fig. 11. In Fig. 12 we compare our results for the bulk states (the 12-V curve of Fig. 7) with two possible approximations. In the first we integrate through the zone of occupied states using a weight function which is unity if the state when photoexcited can escape the material and zero otherwise. This approximation is clearly analogous to the assumption that photoemission reflects only the density of states.[4] For the second estimate we proceed as in the first except that instead of setting the weight to unity we use the Lorentzian

$$\frac{\Gamma}{(E_{\vec{k}}^{f} - E_{\vec{k}}^{b} - \hbar\omega)^2 + \Gamma^2} \quad , \tag{56}$$

where $E_{\vec{k}}^{b}$ is the energy of the occupied bulk state [Eq. (43)] and $E_{\vec{k}}^{f}$ is the free-electron energy for the *same* reduced momentum which can escape the material. Quite arbitrarily we choose the width Γ to be 0.25 eV. Our only aim here is to reflect
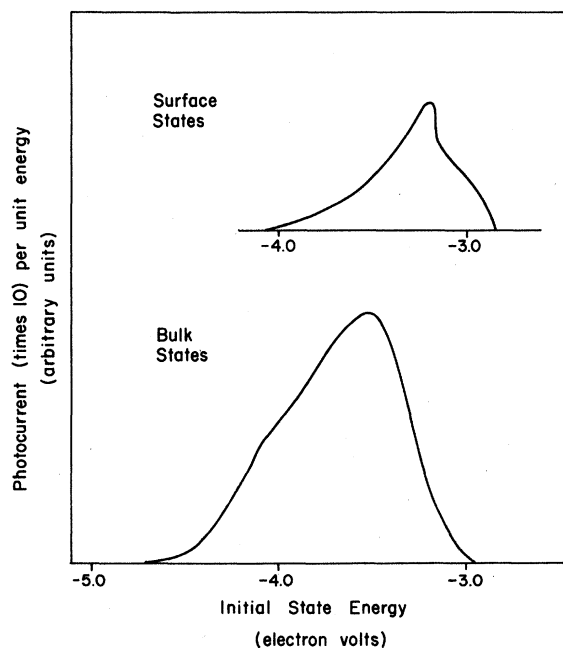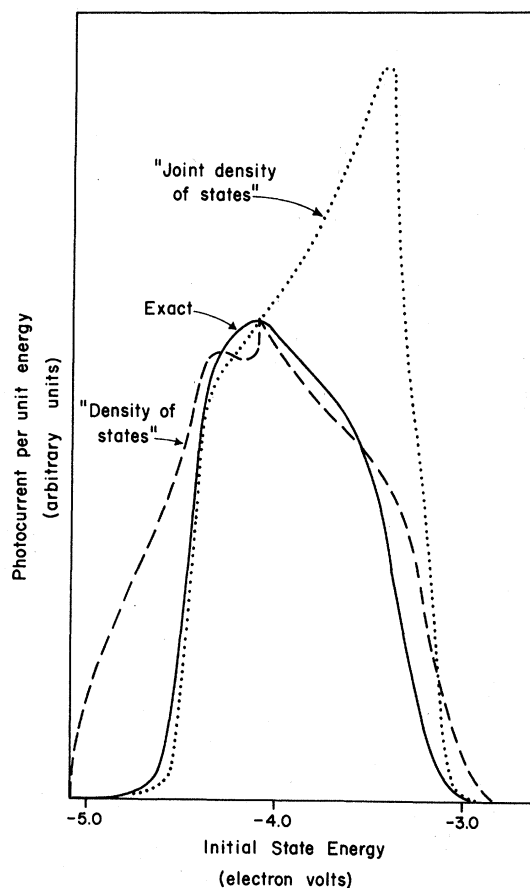

FIG. 11. EDC's for Goodwin model for unit photon flux at normal incidence. The photon energy is 12 eV; the units on the ordinate are the same as in Fig. 7 but note carefully that the photocurrent has been multiplied by a factor of 10 before plotting.

the distribution of the *joint density of states*.[34,31] In Fig. 12 we have scaled the two approximate results to facilitate comparison. Each curve has its own special characteristics. Suprisingly the data with the least structure are those which include the matrix elements. For instance, the "density-of-states" curve shows a sharp cusp associated with the electrons from the momentum region around $(\pi/a, 0, 0)$.[40] From Eq. (40) we see that when $k_x \approx \pi/a$, the occupied state possesses a node at the surface and hence for transitions from these states the oscillator strength is weakened. As for the disagreement at lower energies (from -5.1 to -4.5 eV here), this demonstrates the importance of momentum conservation in the description of the photoemission from these particular bulk states as well as another nodal effect near $\vec{k} = 0$. The curve based on the joint density of states does follow more closely the exact result in this energy range. However, it has an anomalous and quite pronounced structure at higher energies (-3.5 eV). We feel that this is the result of an incipient logarithmic singularity[41] whose contributing states cannot all escape after photoexcitation. Note, for instance, the appearance of a high-energy shoulder on the bulk-state yield when the work function is lowered, Fig. 8. However, application of the joint-density-of-states approximation in this case increases even more the anomalous structure. Some progress toward understanding why this structure is lost in the exact curve can be made by noting that the photoelectrons which contribute in this energy range emerge obliquely from the material. Accordingly their normal momenta $[\hbar f$ of Eq. (20)] are rather small. Since we have used a step barrier at the surface in forming the final states, our transmission factor[10,42]

$$T = 4f \, K_x/(f + K_x)^2 \qquad (57)$$

vanishes as $f \to 0$. A more realistic model would perhaps use an image potential barrier[43] for which the transmission factor is essentially unity at all energies above vacuum.[44,45] To simulate this correction we repeat the exact calculation except for the replacement

$$T \to T_{\text{approx}} = \frac{4f K_x}{(f + K_x)^2} \frac{1}{\cos\theta} \, . \qquad (58)$$

Since

$$f = (2mE/\hbar^2)\cos\theta \, , \qquad (59)$$

T_{approx} is finite at zero normal momentum. In Fig. 13 we compare this curve with the joint-density-of-states approximation of Fig. 12. The qualitative agreement is considerably improved. It is possible that much of the remaining discrepancy may represent a further matrix element effect since the
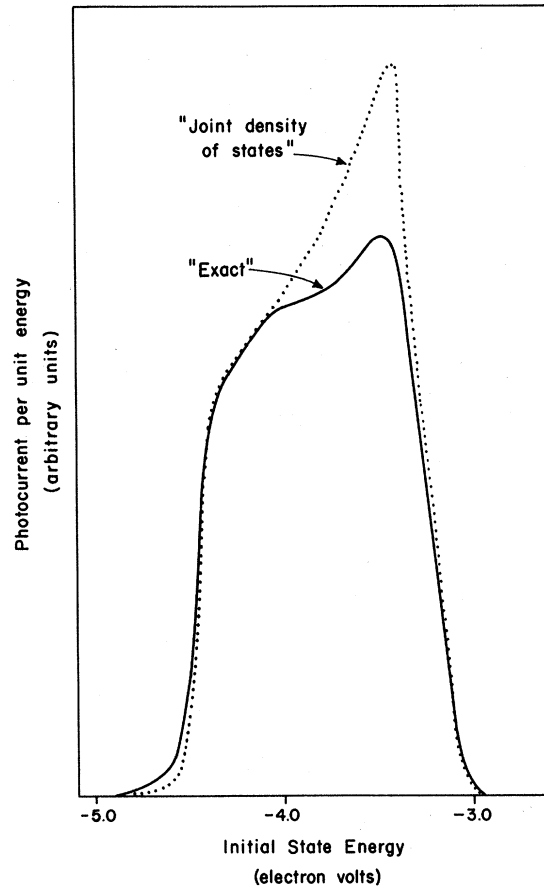

FIG. 13. EDC's for goodwin model in various approximations plotted as in Fig. 12. Full curve: exact result except for approximate transmission factor of Eq. (58); dotted curve: joint-density-of-states approximation.

contributing photoelectrons come from bulk states near the plane $k_x \approx \pi/a$ and hence have surface nodes. Our conclusion is simply that matrix element effects can mask the agreement of photoemission data with the predictions based on the joint density of states.

We close this section with some brief comments on an attempt to modify Goodwin's model. We have considered the possibility of incorporating the additional complications inherent in an fcc lattice with again a {100} face exposed to vacuum. It is straightforward to determine the eigenfunctions but unfortunately the density of states contains a logarithmic singularity at the upper edge associated with the degeneracy on the X face of the conventional Brillouin zone.[46] Although in this model the high-energy edge of the EDC (when plotted against initial energy) is stationary as photon energy is varied, we feel that the singular behavior at this edge (though it is removed by matrix element effects: surface nodes) renders further calculation inadvisable.

V. DISCUSSION

The results that we have presented above indicate the difficulty of a realistic calculation, even in the independent-particle approximation, of the photoemission from real metals. Apart from the considerable problem of optical absorption, there is the complication of the presence of a surface which introduces standing waves and transmission factors which may strongly modify matrix elements. Since the proper description of the surface region is of significant numerical consequence, several aspects of the present calculations must be improved before attempting detailed comparison with experiment. The single-particle potential in the surface region must be more carefully described, including specifically an image potential barrier and appropriate allowance for surface roughness. In addition the behavior of the radiation field in the surface region requires precise description since it scales the yield for surface effects and contributes to the polarization dependence of the photoemission.[47]

On the other hand, we remark that the sensitivity of the calculation contains the promise of much valuable information. Various models of metal surfaces could possibly be distinguished and surface perturbations could be studied. This last point is, however, limited in our formalism to the retention of transverse periodicity.[48] We can write from Eq. (4) an expression for the photocurrent in the more general case—essentially it involves a trace over three single-particle current operators—but as yet we do not know how to proceed from there. With this limitation in mind, we would urge experimentalists to obtain photoemission data from single-crystal faces in order to facilitate analysis. There would still be the disordering influence of phonon scattering and surface roughness with which to contend but these effects could hopefully be minimized with sufficient care.

*Work supported by NSF Grant No. GP-14802. Portions of this work are based on a thesis by W. Schaich submitted to the Faculty of the Graduate School of Cornell University, 1970 (unpublished) (Materials Science Center Report No. 1403).

†NSF Predoctoral Fellow; present address: H. H. Wills Physics Laboratory, Royal Fort, Tyndall Avenue, Bristol, England. The support of an AFOSR-NRC Fellowship during the final stages of this work is gratefully acknowledged.

[1] A. Einstein, Ann. Physik 17, 132 (1905).

[2] G. W. Gobeli et al., Phys. Rev. Letters 12, 94 (1964).

[3] E. O. Kane, Phys. Rev. Letters 12, 97 (1964).

[4] C. N. Berglund and W. E. Spicer, Phys. Rev. 136, A1030 (1964).

[5] C. N. Berglund and W. E. Spicer, Phys. Rev. 136, A1044 (1964).

[6] N. W. Ashcroft and W. L. Schaich, in Proceedings of the Density of States Symposium, National Bureau of Standards, 1969 (unpublished).

[7] G. Mahan, Phys. Rev. Letters 24, 1068 (1970); and Phys. Rev. B (to be published).

[8] K. Mitchell, Proc. Roy. Soc. (London) A146, 442 (1934).

[9] R. de L. Kronig and W. G. Penney, Proc. Roy. Soc. (London) A130, 449 (1931).

[10] W. Schaich and N. W. Ashcroft, Solid State Commun. 8, 1959 (1970).

[11] W. Schaich, thesis, Cornell University, Ithaca, N. Y., 1970 (unpublished) (Materials Science Center Report No. 1403).

[12] R. Kubo, J. Phys. Soc. Japan 12, 570 (1957).

[13] We have written the result for only the normal component of the current density since this is the experimentally measured quantity if the detector collects all electrons that emerge within a given solid angle. See Ref. 11 for further discussion.

[14] More care is required for the case of an image potential. See K. Mitchell, Proc. Cambridge Phil. Soc. 31, 416 (1935).

[15] I. Adawi, Phys. Rev. 134, A788 (1964).

[16] A. Messiah, Quantum Mechanics (North-Holland, Amsterdam, 1966), p. 802.

[17] L. I. Schiff and L. H. Thomas, Phys. Rev. 47, 860 (1935).

[18] R. E. B. Makinson, Proc. Roy. Soc. (London) A162, 367 (1937).

[19] This result, found, for example, in H. A. Bethe and E. E. Salpeter [Quantum Mechanics of One and Two Electron Atoms (Academic, New York, 1957)], was first applied to photoemission by I. Adawi, Ref. 15.

[20] R. E. B. Makinson, Phys. Rev. 75, 1908 (1949).

[21] The Fermi momentum is determined from the free-electron dispersion relation.

[22] M. J. G. Lee, Proc. Roy. Soc. (London) A295, 440 (1966).

[23] N. V. Smith and W. E. Spicer, Phys. Rev. 188, 593 (1969).

[24] A. H. Wilson, Theory of Metals (Cambridge U. P., Cambridge, England, 1958), 2nd ed., p. 25.

[25] The numerical data of Ref. 6 had a slight error which is corrected here. It leads to no qualitative change.

[26] K. Mitchell, Proc. Roy. Soc. (London) A153, 513 (1935).

[27] F. J. Piepenbring, in Optical Properties and Electronic Structure of Metals and Alloys, edited by F. Abeles (North-Holland, Amsterdam, 1966), p. 316.

[28] J. A. Strozier and R. O. Jones, Phys. Rev. Letters 22, 1186 (1969); and (unpublished).

[29] B. I. Lundqvist, Phys. Status Solidi 32, 273 (1969).

[30] Note that the neglect of the variation of the vector potential (optical absorption) with photon energy is a

clearly unrealistic procedure here.

[31]N. V. Smith and R. Y. Koyama (unpublished).

[32]E. T. Goodwin, Proc. Cambridge Phil. Soc. 35, 205 (1939). We modify his model [following A. Many et al., Semiconductor Surfaces (North-Holland, Amsterdam, 1965), p. 174, whose notation we adopt] to refer to a semi-infinite crystal rather than one of N layers.

[33]D. Beaglehole and E. Erlbach, Solid State Commun. 8, 255 (1970).

[34]N. V. Smith, in Ref. 6.

[35]W. F. Krowlikowski and W. E. Spicer, Phys. Rev. 185, 882 (1969).

[36]The strong growth in width on the high-energy side of the bulk-state yield is another misleading aspect of the model.

[37]F. Forstmann and V. Heine, Phys. Rev. Letters 24, 1419 (1970).

[38]F. Forstmann and J. B. Pendry, Z. Physik 235, 75

(1970).

[39]The data for $b = \frac{3}{4}a$ were essentially identical (somewhat below) those for $b = \frac{1}{2}a$..

[40]The reason for the difference between this curve and the one of Fig. 6 is that we have imposed the condition of escape after excitation.

[41]E. O. Kane, Phys. Rev. 175, 1039 (1968).

[42]A. Messiah, Ref. 16, p. 106.

[43]C. Herring and M. H. Nichols, Rev. Mod. Phys. 21, 185 (1949).

[44]L. A. MacColl, Phys. Rev. 56, 699 (1939).

[45]L. A. MacColl, Bell System Tech. J. 30, 888 (1951).

[46]N. F. Mott and H. Jones, Properties of Metals and Alloys (Dover, New York, 1958), p. 68.

[47]M. Skibowski et al., Z. Physik 211, 343 (1968); S. V. Pepper, J. Opt. Soc. Am. 60, 805 (1970).

[48]Some progress is possible in perturbation theory; see Ref. 10.

Doppler-Shifted Acoustic Cyclotron-Resonance Studies in Magnesium[†]

R. W. Stark

The James Franck Institute and the Department of Physics,
The University of Chicago, Chicago, Illinois 60637
The University of Arizona, Department of Physics, Tucson, Arizona 85721

and

J. Trivisonno and R. E. Schwarz

The Department of Physics, John Carroll University, Cleveland, Ohio 44118
(Received 12 October 1970)

A study of Doppler-shifted acoustic cyclotron resonance in magnesium is reported. The results are compared with the quantitative predictions of band-structure calculations based on the nonlocal orthogonalized-plane-wave pseudopotential model Hamiltonian for magnesium reported by Kimball, Stark, and Mueller. The dominant family of resonances yield an experimental value for the rate of change of the cross-sectional area of the Fermi surface with the component of the electron wave vector along the magnetic field of 0.80 ± 0.02 a.u. compared with a theoretical prediction of 0.793 a.u. The experimental cyclotron mass of 0.78 ± 0.05 free-electron masses compares with a prediction of 0.78 ± 0.02 free-electron masses. The expectation value of the electron drift velocity along the magnetic field determined from experiment is 3.65×10^7 cm/sec, while theory predicts 3.73×10^7 cm/sec. The relative amplitudes of the successive resonances in the attenuation are in the ratio $1:0.64:0.41$ compared with a predicted ratio of $1:0.645:0.344$. At $4.2\,°K$ the electron mean free path for small-angle scatter determined from the resonance line shape was 1.4 mm compared with a sample thickness of 1.9 mm. At the lowest temperatures used with the experiment, the mean free path becomes equivalent to the sample thickness.

I. INTRODUCTION

The attenuation of a sound wave in a pure metal at low temperatures is dominated by the interaction of the wave with the conduction electrons. The first conclusive experimental evidence for the importance of the role played by the conduction electrons was the observation of a sharp reduction in the attenuation upon crossing the transition from the normal state into the superconducting state.[1,2] Shortly after the initial observations it was found that the

attenuation could be effected in a nonmonotonic way by the application of a magnetic field of varying strength and orientation.[3]

Various aspects of the physical manifestations of the interaction of sound waves with electrons orbiting in the presence of an applied magnetic field $\vec{H}$ have been discussed in some detail by several authors.[4-7] The phenomenon of "geometric resonance" has been extensively utilized to determine dimensions of Fermi surfaces.[8] In that experiment, $\vec{H}$ is applied perpendicular to the sound